Localized and Collective Motions in HET-s(218-289) Fibrils from Combined NMR Relaxation and MD Simulation

Albert A. Smith, Matthias Ernst,* Sereina Riniker,* and Beat H. Meier*

Abstract: *Nuclear magnetic resonance (NMR) relaxation data and molecular dynamics (MD) simulations are combined to characterize the dynamics of the fungal prion HET-s(218-289) in its amyloid form. NMR data is analyzed with the dynamics detector method, which yields timescale-specific information. An analogous analysis is performed on MD trajectories. Because specific MD predictions can be verified as agreeing with the NMR data, MD was used for further interpretation of NMR results: for the different timescales, cross-correlation coefficients were derived to quantify the correlation of the motion between different residues. Short timescales are the result of very local motions, while longer timescales are found for longer-range correlated motion. Similar trends on ns- and µs-timescales suggest that µs motion in fibrils is the result of motion correlated over many fibril layers.*

Nuclear magnetic resonance (NMR) is a sensitive tool for the characterization of timescale-specific motion in proteins. Relaxation-rate constants probe the re-orientation of internuclear vectors (for example, the ^{1}H–^{15}N bond), which is the result of possibly complex motional processes.[1] For simple motions, described by a single correlation time and amplitude, measurement of relaxation-rate constants yields information on both parameters. Even for such simple models, the degree of correlation of motion over several bonds is not easily assessed (although cross-correlations of nearby bonds can be obtained in solution-state NMR[2]). With more complex motions, characterized by multiple correlation times and amplitudes, the disentanglement of amplitudes and correlation times becomes increasingly ambiguous.[3] Furthermore, it is not straightforward to connect local bond motions to overall motions, which involve the correlated motion of many nuclei. These difficulties prevent the visualization of motional processes from the NMR data in the form of movies.

Molecular dynamics (MD) simulations naturally provide such movies and statistical correlations. However, the predictions are limited by trajectory length and quality of the force field, so resulting dynamics should be validated by experiments.[4] It is, therefore, attractive to combine MD and NMR to interpret the NMR data in terms of more complex overall motions.

Comparison between NMR and MD can be made at the level of relaxation-rate constants by calculating these from MD trajectories,[5] or at the level of amplitudes and correlation times obtained by modeling the correlation function of the H–N bond as a sum of a few exponentials[6] (for example, the model-free approach[7]). The former can give good agreement, but it is less intuitive, while the latter often leads to incompatible results owing to ambiguities mentioned above.

Therefore, we compare NMR and MD in terms of the detector approach.[3] For a quantitative, timescale-specific motional analysis, we analyze the NMR relaxation data using the detector approach and then apply it to MD trajectories to obtain amplitudes of the same detectors. For HET-s(218-289) fibrils,[8] we find good agreement using the AMBER 99SB-ILDN force field[9] in a 500 ns simulation. Correlation analysis determines how detector responses on different timescales are related to overall motion: similar amplitude trends are found on a wide range of timescales, but these trends at short correlation times result from more local motions, while for longer times they result from collective motions over multiple fibril layers. A detector-specific (that is, timescale-specific) correlation coefficient is derived from MD data, which is used to relate NMR-based localized H–N motions to overall motion. Despite fibrils being fairly rigid, a very wide range of correlation times was detected, which results from motion with different correlation lengths.

Nine previously acquired NMR experiments[10] were used to characterize backbone H–N bond motion of HET-s(218-289) in amyloid form ($3R_1$, $5R_{1\rho}$ rate constants and order parameters). Previous analysis assumed that the correlation function of the bond motion is a sum of three discrete exponential terms,[6b,c] each described by an order parameter (S^2) and correlation time (τ_c). Upon closer inspection, we found the fitted τ_c can be biased by this approach, and depend strongly on the set of experiments used.[3a] We suspect this is a near-universal problem when complex motions are involved, brought about by fitting a correlation function with fewer terms than are present in the real motion. Further evidence of biasing is provided in the Supporting Information,

[*] Dr. A. A. Smith, Prof. Dr. M. Ernst, Prof. Dr. S. Riniker, Prof. Dr. B. H. Meier
Physical Chemistry, ETH Zurich
Vladimir-Prelog-Weg 2, 8093 Zurich (Switzerland)
E-mail: maer@ethz.ch
sriniker@ethz.ch
beme@ethz.ch

Dr. A. A. Smith
Present address: Institut für Medizinische Physik und Biophysik
Universität Leipzig
Härtelstraße 16–18, 04107 Leipzig (Germany)

Supporting information and the ORCID identification number(s) for the author(s) of this article can be found under:
https://doi.org/10.1002/anie.201901929.

Section 4, where we find that an MD trajectory yields good reproduction of experimental R_1 rate constants at several magnetic fields, but fitting of NMR data and MD-derived correlation functions separately to multi-exponential functions yields very different parameters (see [5d] for similar results for methyl dynamics).

To compare MD and NMR analyses, we must allow for complex motional models; detectors use an arbitrary number of correlation times in the correlation function,[3] given as:

$$C(t) = S^2 + (1-S^2) \int_{-\infty}^{\infty} \theta(z)\exp(-t/(10^z \cdot 1\,\mathrm{s}))\mathrm{d}z \quad (1)$$

$(1-S^2)\theta(z)$ is a distribution of motion, where $\theta(z)$ integrates to one, and $(1-S^2)$ scales the distribution. Integration sums contributions for all correlation times ($\tau_c = 10^z \cdot 1\,\mathrm{s}$) to obtain $C(t)$. The distribution can assume any functional form: for example, for one correlation time, τ_c, and order parameter, S^2, the distribution is $(1-S^2)\delta(z-\log_{10}(\tau_c))$, where $\delta(z)$ is the delta function. However, a continuous distribution is also possible, where such a distribution may be described with a few parameters,[11] or it may have an entirely arbitrary form.

We cannot fully determine $(1-S^2)\theta(z)$ without assumptions about its form, but we may characterize ranges of correlation times, with ranges defined by detector sensitivities $\rho_n(z)$ (Figure 1A). Motion in the range of $\rho_n(z)$ is obtained as:[3]

$$\rho_n^{(\theta,S)} = (1-S^2) \int_{-\infty}^{\infty} \theta(z)\rho_n(z)\mathrm{d}z \quad (2)$$

$\rho_n^{(\theta,S)}$, the detector response, is the weighted average of the distribution, $(1-S^2)\theta(z)$, where $\rho_n(z)$ is the weighting function (assuming detectors are integral-normalized, $\int\rho_n(z)\mathrm{d}z = 1$). The $\rho_n(z)$ are linear combinations of spectral-density functions, optimized to be as narrow as possible, and the corresponding detector responses are linear combinations of experimental rate constants. Each detector has a center and width on a $\log_{10}$ scale (for example, ρ_1 has center $z_1^0 = -9.1$, $10^{z_1^0} \approx 700\,\mathrm{ps}$, and width $\Delta z_1 = 1.2$, or just over an order-of-magnitude). If $(1-S^2)\theta(z)$ is approximately linear over the sensitive range of a detector, $\rho_n^{(\theta,S)}$ approximates the distribution at the detector center, $z = z_n^0$.[3b] Although the $\rho_n^{(\theta,S)}$ do not allow reconstruction of $C(t)$, they are well defined and describe the information in the NMR data with reduced experimental bias (further discussion on detector interpretation in given in the Supporting Information, Section 2).

We can also obtain $C(t)$ from an MD trajectory,[12] invert Equation (1) to obtain $(1-S^2)\theta(z)$, and insert the result into Equation (2), to obtain $\rho_n^{(\theta,S)}$ (calculating $(1-S^2)\theta(z)$ is an ill-posed problem, but this does not create significant problems when calculating; Supporting Information, Section 3).

Figure 1B shows $\rho_n^{(\theta,S)}$ for backbone H−N motion of HET-s(218-289) fibrils. These experimental responses depend, to excellent approximation, only on R_1 relaxation data at 400, 500, and 850 MHz and order parameters.[10] MD responses are based on a 500 ns trajectory of a stretch of fibril with 3 HET-
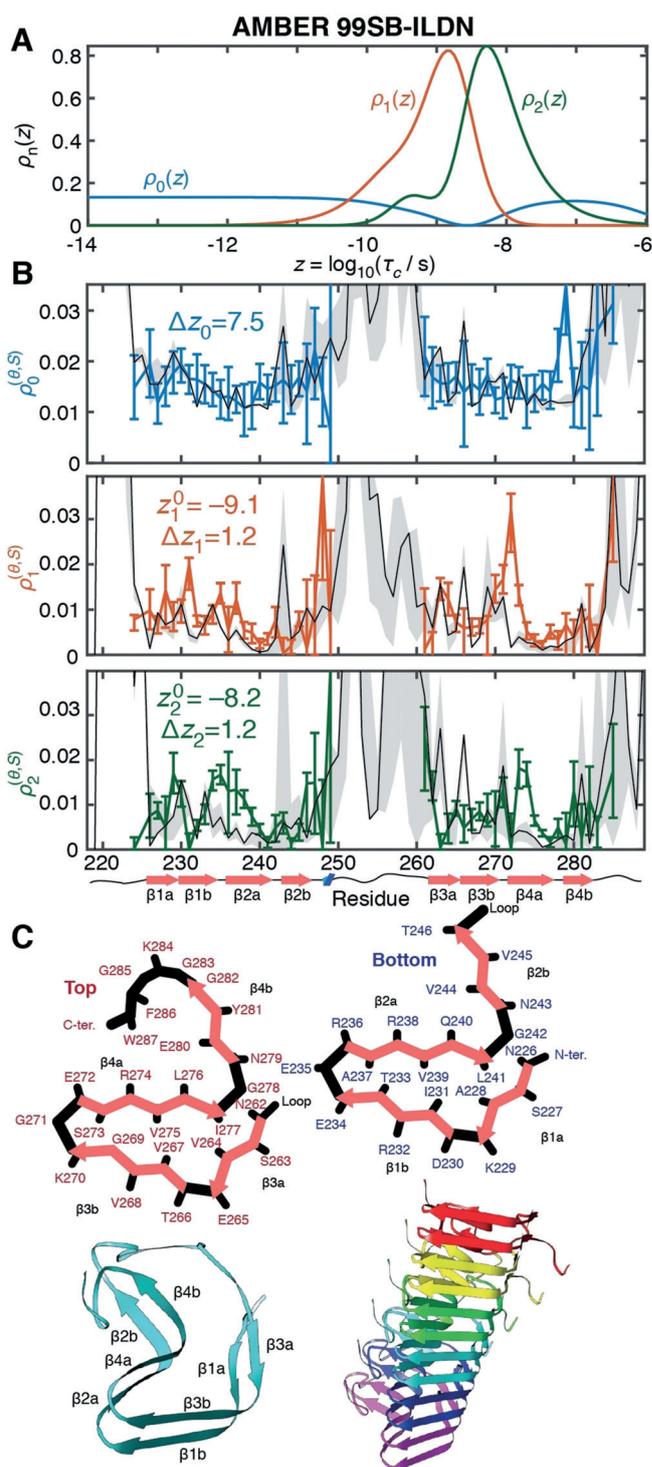

Figure 1. NMR and MD detector responses for HET-s(218-289) fibrils. A) plots $\rho_n(z)$ for $\rho_0-\rho_2$ (see the Supporting Information, Figure S1 for the full range). B) Responses derived from experiment (color with error bars) and MD simulation (black). The gray area estimates a confidence interval for MD results, obtained by analyzing the first and second halves of the trajectory separately, and plotting the range of results. z_n^0 and Δz_n give centers and widths of the $\rho_n(z)$ (log scale[3b]). C) HET-s(218-289) β-sheet arrangement, 3D views of a single HET-s molecule, and 6 molecules in a fibril. One molecule forms two layers connected by a flexible loop.

s(218-289) molecules (6 fibril layers, AMBER 99SB-ILDN force field;[9] see the Supporting Information, Section 1.2 for setup[13]). $R_{1\rho}$ data is simultaneously processed with R_1 data, but because $R_{1\rho}$ is far more sensitive to µs motions than ns motions (Supporting Information, Figure S1), they result in two additional µs detectors (discussed later), which cannot be directly compared to a 500 ns trajectory.

ρ_0 is primarily sensitive to short correlation times, representing vibrational and librational motions. From experiment alone, it is not clear if slower motion ($\tau_c \approx 100$ ns, Figure 1 A) might also contribute to ρ_0. We can separate motions with greater resolution using MD, where results show that fast motions (< 100 ps) dominate ρ_0 in β-sheets (Supporting Information, Section 5.1). We see fairly uniform behavior throughout the molecule for experimental results, and have good reproduction by MD (Figure 1 B). The reference bond length is optimized for detector analysis to a length of 1.03 Å (Supporting Information, Section 3.4). Bond lengths are motionally averaged; including more motions (for example, librations, stretching) increases the effective length, and reduces $\rho_0^{(\theta,S)}$. While 1.01 Å corresponds to the minimum energy of the H−N bond, effective lengths can range from 1.02–1.04 Å, depending on which motions are averaged to determine the effective length.[14]

ρ_1 and ρ_2 are the two detectors ($10^{z_1^0} \approx 700$ ps, $10^{z_2^0} \approx 6$ ns) characterizing motions relevant for R_1 relaxation. For ρ_1 and ρ_2, MD and NMR show similar increases in motion near the flexible loop (260–270, the loop itself is invisible in spectra), for β1a, and for β1b and β3b near the turns between β-sheets (E235 and G271). Motion on β2a and β4a is underestimated by MD. Overall, for both ρ_1 and ρ_2 agreement between MD and NMR is good, with trends and the absolute amplitudes of $\rho_1^{(\theta,S)}$ and $\rho_2^{(\theta,S)}$ reproduced, without using adjustable parameters. Disagreement can have a number of causes, including limited sampling with MD and incorrect reproduction of dynamics by the force field. The former may lead to higher residue-to-residue variation observed for MD. The GROMOS 54a7[15] force field yields less agreement (Supporting Information, Figure S7; see Ref. [16] for comparison of force-field families).

We want to correlate measured $\rho_n^{(\theta,S)}$ of the H−N bonds with surrounding motion using MD data. Standard methods exist to correlate motion of bond pairs,[17] but typically do not have timescale specificity (other approaches also exist[14d]). Therefore, we define a detector-specific (that is, timescale-specific) correlation coefficient. Suppose we take two vectors in the molecule (for example, bonds), indexed k and j. We may calculate a time-correlation function between the vectors, $C_{k,j}(t)$ ($C_{k,j}(t)$ is a tensor correlation function, and has a rank, for example, 1 or 2).[12b] As in Equation (1), $C_{k,j}(t)$ can be fitted with a distribution, $\theta_{k,j}(z)$ (Supporting Information, Section 6.1). Then, the cross-correlated detector response is defined similarly to Equation (2):

$$\rho_n^{k,j} = \int_{-\infty}^{\infty} \theta_{k,j}(z)\rho_n(z)\mathrm{d}z \qquad (3)$$

The cross-correlated response is defined using the same sensitivity, $\rho_n(z)$, as is used to obtain the detector response

$\rho_n^{(\theta,S)}$, so cross-correlation is obtained for exactly the same range of correlation times to which $\rho_n^{(\theta,S)}$ is sensitive. Then, we can determine how the $\rho_n^{(\theta,S)}$ are related to surrounding motion. For easier interpretation, we normalize $\rho_n^{k,j}$ to yield a correlation coefficient:[18]

$$\rho_{n,\text{norm}}^{k,j} = \frac{\rho_n^{k,j}}{\sqrt{\rho_n^{k,k}\rho_n^{j,j}}} \qquad (4)$$

$\rho_{n,\text{norm}}^{k,j}$ can be between 1 (fully correlated) and −1 (fully anti-correlated), or 0 for no correlation. $\rho_{n,\text{norm}}^{k,j}$ also depends on the orientation of the two vectors; we calculate rank-1 correlations in the main text to obtain a simpler angular dependence on correlations, although rank-2 correlation may also be used (in which case $\rho_n^{k,K} = \rho_n^{(\theta,S)}$). Using rank-1, correlated motion may yield −1 in the case that the vectors point in opposite directions and yield 0 for perpendicular vectors (Supporting Information, Section 6.2). Note that we perform the above calculations with an eigenmode approach (iRED[19]) that yields faster and more stable results (Supporting Information, Section 6.3).

To test the behavior of $\rho_{n,\text{norm}}^{k,j}$, we calculate cross-correlation of H-N motion with peptide plane motion (we correlate to a vector in the peptide plane: the bisector of the C′−N and C′−Cα bonds). We expect H−N motion to be highly correlated with peptide plane motion, except for librational motion of the H−N out of the peptide plane. Since this is a fast motion, found in the sensitive range of ρ_0, one expects reduced correlation for ρ_0, but high correlation for ρ_1 and ρ_2. In Figure 2, we see that the behavior of $\rho_{n,\text{norm}}^{k,j}$ is as expected; correlation in the sensitive range of ρ_0 ranges from about 60–95 %, but for ρ_1 and ρ_2, correlation is always higher (> 80 %).

Next, we determine how H−N bond motions are correlated with the motion of the surrounding residues, by calculating correlation coefficients between all backbone H−N bonds. In Figure 3, the correlation between H−N bonds of 232Arg, 235Glu, and 248Ala to H−N bonds of all other
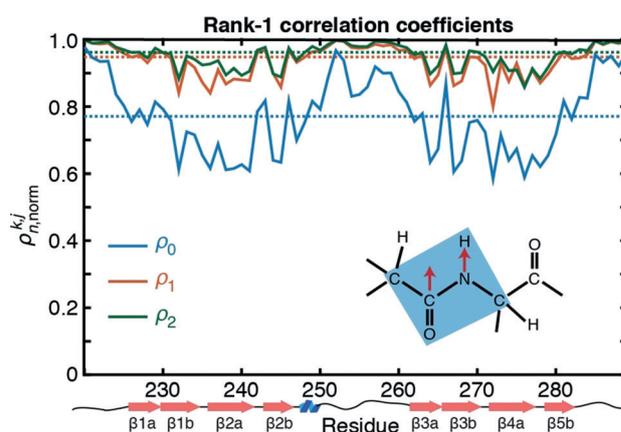

Figure 2. Detector-specific correlation of motion between H−N bonds and peptide planes. $\rho_{n,\text{norm}}^{k,j}$ [Eq. (4)] is plotted for each residue. The inset (lower right) shows the vectors being correlated. For the equivalent rank-2 calculation, see the Supporting Information, Figure S15.
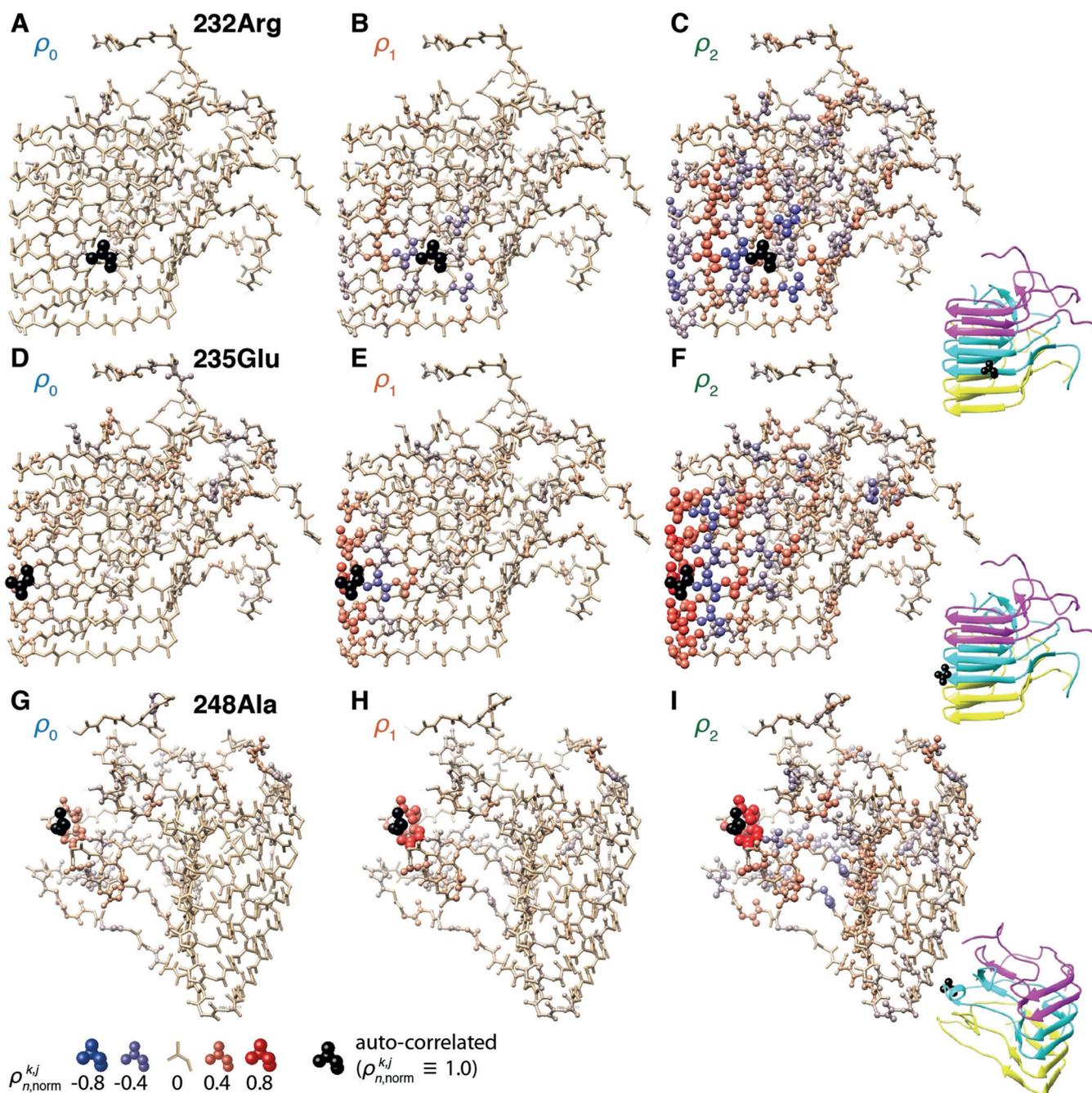
Figure 3. Detector-specific H−N correlation coefficients for several residues. Each subplot shows 6 fibril layers (3 molecules). A)–C) $\rho_{n,norm}^{k,j}$ between the 232Arg H−N bond of the middle HET-s(218-289) molecule (black) to all other H−N bonds, for ρ_0–ρ_2. Atom volumes are proportional to $|\rho_{n,norm}^{k,j}|$, and color coding also indicates the sign. Atoms in the same peptide plane as the H−N bond are also sized and colored according to $\rho_{n,norm}^{k,j}$. D)–F) Correlation for 235Glu; G)–I) correlation for 248Ala. Usually, anti-correlation indicates concerted β-sheet motion, where neighboring residues have H−N bonds pointing opposite directions (Supporting Information, Section 6.2). Small fibril plots (right) show the fibril structure and orientation (all molecular graphics from UCSF Chimera[20]).

residues is plotted (see also the Supporting Information, Figure S20). In the sensitive range of ρ_0, only weak correlation is seen to neighboring residues. For ρ_1 ($10^{z_1^0} \approx 700$ ps), 232Arg shows correlation primarily to residues in the same β-sheet (β1b), whereas for ρ_2 ($10^{z_2^0} \approx 6$ ns), correlation to 232Arg H−N motion is extensive, with strong correlation in the same β-sheet and also two fibril layers away. 235Glu shows similar behavior, where the correlation length increases with corre-

lation time. 248Ala behavior differs; it is highly correlated to 247Ala and 249Ala (with limited correlation for ρ_0), but does not become as correlated with distant residues in the range of ρ_2. This is likely due to more flexibility; since these residues are not hydrogen-bonded in the fibril core their motion is not highly correlated over multiple fibril layers. These behaviors are seen throughout the fibril (complete results in the Supporting Information, Figures S16–S21, including noise

analysis). Similar results are found using the GROMOS force-field (Supporting Information, Figures S22–S25).

The relationship between correlation time and the inter-residue distance of the observed correlations suggests that longer-range motions (> 5 layers) may occur at longer correlation times (about µs range). We cannot verify this with our current MD trajectory; we are limited by both its length and number of fibril layers. We can use $R_{1\rho}$ relaxation, which has been established as a reliable reporter on micro-second dynamics,[21] to calculate detectors sensitive to µs motion, and compare to $\rho_1^{(\theta,S)}$ and $\rho_2^{(\theta,S)}$. Figure 4B shows detector responses sensitive in the µs range ($10^{z_3^0} \approx 2$ µs, $10^{z_4^0} \approx 20$ µs), and C compares them to ns-range detectors ($\rho_0^{(\theta,S)}$ is relatively uniform, so is not shown in C). Responses are significantly lower than in Figure 1, but have similar trends: increased amplitude near the loop and C-terminus, and increases between β1b/β2a and β3b/β4α. Similarity of $\rho_n^{(\theta,S)}$ around the ns and µs regimes can be because the

underlying motion is similar, with the primary difference being the correlation length, which leads to an increase in correlation time. Such behavior has been observed in polymer dynamics, where motional modes involving a few or many monomers lead to short and long correlation times,[22] and, furthermore, these modes have also decreasing amplitudes with increasing correlation times.

From these results, we can therefore partially characterize the origin of the multi-timescale motion in HET-s(218-289) fibrils: increased correlation length brings about longer correlation times on the ns timescale, and we suspect this trend can be extended to explain the observed µs dynamics, pointing to broad distributions of correlation times. This behavior could be related to the small-amplitude µs rocking motion observed even in crystalline proteins such as ubiquitin, GB1, and SH3[21c,23] or it could be a different type of fibril motion. Presence of strong interactions between molecules in both fibrils and protein crystals can yield motions involving multiple molecules (where it is not clear if weaker interactions between neighboring fibrils might also contribute). We believe that this type of motion, however, is best described by a distribution of correlation times, as opposed to a single effective correlation time.

The combination of NMR and MD using the detector approach allows us to draw conclusions neither of the two methods would provide on its own. Such an approach can be used to characterize collective motions critical for biological function.

Conflict of interest

The authors declare no conflict of interest.

Figure 4. Detectors sensitive to µs motion (ρ_3: $10^{z_3^0} \approx 2$ µs, ρ_4: $10^{z_4^0} \approx 20$ µs). A) Plots of $\rho_3(z)$ and $\rho_4(z)$. B) plots responses, $\rho_n^{(\theta,S)}$ (cut-off values are visible in the Supporting Information Figure S26). C) Maps $\rho_n^{(\theta,S)}$ for $\rho_1-\rho_4$ onto the HET-s(218–289) molecule (data from Figure 1B, Figure 4B). $\rho_n^{(\theta,S)}$ above the scale are omitted (scale above each molecule.)

[1] a) K. Henzler-Wildman, D. Kern, *Nature* **2007**, *450*, 964–972;
b) J. R. Lewandowski, M. E. Halse, M. Blackledge, L. Emsley, *Science* **2015**, *348*, 578.

[2] P. Pelupessy, S. Ravindranathan, G. Bodenhausen, *J. Biomol. NMR* **2003**, *25*, 265–280.

[3] a) A. A. Smith, M. Ernst, B. H. Meier, *Angew. Chem. Int. Ed.* **2017**, *56*, 13590–13595; *Angew. Chem.* **2017**, *129*, 13778–13783;
b) A. A. Smith, M. Ernst, B. H. Meier, *J. Chem. Phys.* **2018**, *148*, 045104.

[4] a) W. F. van Gunsteren, X. Daura, N. Hansen, A. E. Mark, C. Oostenbrink, S. Riniker, L. J. Smith, *Angew. Chem. Int. Ed.* **2018**, *57*, 884–902; *Angew. Chem.* **2018**, *130*, 894–915; b) D. A. Case, *Acc. Chem. Res.* **2002**, *35*, 325–331; c) P. Bernadó, K. Modig, P. Grela, D. I. Svergun, M. Tchorzewski, M. Pons, M. Akke, *Biophys. J.* **2010**, *98*, 2374–2382.

[5] a) L. Mollica, M. Baias, J. R. Lewandowski, B. J. Wylie, L. J. Sperling, C. M. Rienstra, L. Emsley, M. Blackledge, *J. Phys. Chem. Lett.* **2012**, *3*, 3657–3662; b) T. Bremi, R. Brüschweiler, *J. Am. Chem. Soc.* **1997**, *119*, 6672–6673; c) S. A. Showalter, R. Brüschweiler, *J. Chem. Theory Comput.* **2007**, *3*, 961–975; d) F. Hoffmann, M. Xue, L. V. Schafer, F. A. A. Mulder, *Phys. Chem. Chem. Phys.* **2018**, *20*, 24577–24590; e) Y. Xue, N. R. Skrynnikov, *J. Am. Chem. Soc.* **2011**, *133*, 14614–14628.

[6] a) G. M. Clore, A. Szabo, A. Bax, L. E. Kay, P. C. Driscoll, A. M. Gronenborn, *J. Am. Chem. Soc.* **1990**, *112*, 4989–4991; b) V. Chevelkov, U. Fink, B. Reif, *J. Biomol. NMR* **2009**, *45*, 197–206; c) P. Schanda, B. H. Meier, M. Ernst, *J. Am. Chem. Soc.* **2010**, *132*, 15957–15967; d) A. G. Palmer III, *Annu. Rev. Biophys. Biomol. Struct.* **2001**, *30*, 129–155; e) J. Chen, C. L. I. Brooks, P. E. Wright, *J. Biomol. NMR* **2004**, *29*, 243–257.

[7] G. Lipari, A. Szabo, *J. Am. Chem. Soc.* **1982**, *104*, 4546–4559.

[8] H. Van Melckebeke, C. Wasmer, A. Lange, E. Ab, A. Loquet, A. Böckmann, B. H. Meier, *J. Am. Chem. Soc.* **2010**, *132*, 13765–13775.

[9] a) K. Lindorff-Larsen, S. Piana, K. Palmo, P. Maragakis, J. L. Klepeis, R. O. Dror, D. E. Shaw, *Proteins Struct. Funct. Bioinf.* **2010**, *78*, 1950–1958; b) V. Hornak, R. Abel, A. Okur, B. Strockbine, A. Roitberg, C. Simmerling, *Proteins Struct. Funct. Bioinf.* **2006**, *65*, 712–725.

[10] A. A. Smith, E. Testori, R. Cadalbert, B. H. Meier, M. Ernst, *J. Biomol. NMR* **2016**, *65*, 171–191.

[11] P. A. Beckmann, *Phys. Rep.* **1988**, *171*, 85–128.

[12] a) B. J. Berne, G. D. Harp, *Adv. Chem. Phys.* **1970**, *17*, 63–227; b) S. F. Lienin, T. Bremi, B. Brutscher, R. Brüschweiler, R. R. Ernst, *J. Am. Chem. Soc.* **1998**, *120*, 9870–9879.

[13] a) J. Dolenc, B. H. Meier, V. H. Rusu, W. F. van Gunsteren, *Phys. Chem. Chem. Phys.* **2016**, *18*, 5860; b) A. Lange, Z. Gattin, H. Van Melckebeke, C. Wasmer, A. Soragni, W. F. Gunsteren, B. H. Meier, *ChemBioChem* **2009**, *10*, 1657–1665.

[14] a) D. A. Case, *J. Biomol. NMR* **1999**, *15*, 95–102; b) M. Ottiger, A. Bax, *J. Am. Chem. Soc.* **1998**, *120*, 12334–12341; c) P. Bernadó, M. Blackledge, *J. Am. Chem. Soc.* **2004**, *126*, 4907–4920; d) K. Kämpf, S. A. Izmailov, S. O. Rabdano, A. T. Groves, I. S. Podkorytov, N. R. Skrynnikov, *Biophys. J.* **2018**, *115*, 2348–2367.

[15] N. Schmid, A. P. Eichenberger, A. Choutko, S. Riniker, M. Winger, A. E. Mark, W. F. van Gunsteren, *Eur. Biophys. J.* **2011**, *40*, 843–856.

[16] S. Riniker, *J. Chem. Inf. Model.* **2018**, *58*, 565–578.

[17] N. Salvi, A. Abyzov, M. Blackledge, *Angew. Chem. Int. Ed.* **2017**, *56*, 14020–14024; *Angew. Chem.* **2017**, *129*, 14208–14212.

[18] K. Pearson, *Proc. R. Soc. London* **1895**, *58*, 240–242.

[19] a) J. J. Prompers, R. Brüschweiler, *J. Am. Chem. Soc.* **2001**, *123*, 7305–7313; b) J. J. Prompers, R. Brüschweiler, *J. Am. Chem. Soc.* **2002**, *124*, 4522–4534.

[20] E. F. Pettersen, T. D. Goddard, C. C. Huang, G. S. Couch, D. M. Greenblatt, E. C. Meng, T. E. Ferrin, *J. Comput. Chem.* **2004**, *25*, 1605–1612.

[21] a) R. Kurbanov, T. Zinkevich, A. Krushelnitsky, *J. Chem. Phys.* **2011**, *135*, 184104; b) J. R. Lewandowski, H. J. Sass, S. Grzesiek, M. Blackledge, L. Emsley, *J. Am. Chem. Soc.* **2011**, *133*, 16762–16765; c) P. Ma, Y. Xue, N. Coquelle, J. D. Haller, T. Yuwen, I. Ayala, O. Mikhailovskii, D. Willbold, J.-P. Colletier, N. R. Skrynnikov, P. Schanda, *Nat. Commun.* **2015**, *6*, 8361; d) P. Rovó, R. Linser, *J. Phys. Chem. B* **2017**, *121*, 6117–6130; e) N. A. Lakomek, S. Penzel, A. Lends, R. Cadalbert, M. Ernst, B. H. Meier, *Chem. Eur. J.* **2017**, *23*, 9425–9433.

[22] a) P. E. J. Rouse, *J. Chem. Phys.* **1953**, *21*, 1272–1280; b) F. n. Vaca Chávez, K. Saalwächter, *Macromolecules* **2011**, *44*, 1560–1569.

[23] A. Krushelnitsky, D. Gauto, D. C. Rodriguez Camargo, P. Schanda, K. Saalwachter, *J. Biomol. NMR* **2018**, *71*, 53–67.